Check for updates

Observational evidence on the coastal upwelling along the northwest coast of India during summer monsoon

Vishnu Narayanan Nampoothiri S ·
Ch. Venkata Ramu · K. Rasheed · Y. V. B. Sarma ·
G. V. M. Gupta

Abstract The lesser known coastal upwelling in the North Eastern Arabian Sea (NEAS) during summer monsoon, its associated dynamics and forcing mechanisms is elucidated for the first time using basin scale monthly time-series in-situ and satellite data. The presence of cool upwelled waters along northwest coast of India from July to early October with an associated increase in productivity was evident in both data. The low level Findlater jet blows towards west coast of India with high wind magnitude (10–12 m/s) during summer monsoon generates strong Ekman transport (1416 kg/m/s) at offshore and Ekman pumping velocity (1.349 m/s) at coastal region initiates upwelling. It was identified that the currents and remote forcing also regulate upwelling along the region. Although upwelling seems to exist along the northwest coast, it was weaker (25.5 °C) compared to the southwest coast where the SST dropped to 24 °C. The upwelling was observed in the south during June as a surface process, while it was observed along the northwest coast of India by the end of August. Even though the onset of upwelling in the NEAS and South Eastern Arabian Sea (SEAS) had a lag of two months, the recession of upwelling happened during late and early September respectively. The cause for the lag in the onset and cessation of upwelling between SEAS and NEAS is attributed to the propagation of Kelvin waves and southwest monsoon winds. The study also reveals that temperature and chlorophyll profiles show bi-modal peaks of high and low associated with winter cooling (winter) and upwelling (summer).

Highlights
- The lesser known coastal upwelling along the NEAS was elucidated for the first time.
- Presence of cooler waters during SM was due to upwelling with an increase in productivity.
- Strong winds (10–12 m/s) generate Ekman transport (1416 kg/m/s) and pumping velocity (1.349 m/s) triggering the upwelling.
- Temperature and chlorophyll profiles shows bi-modal peaks associated with winter cooling and upwelling.
- Change in wind and surface currents and remote forcing are the major forcings.
- Onset of upwelling in the NEAS and SEAS had a lag of two months; the cessation of upwelling occurred simultaneously.

V. Narayanan Nampoothiri S (✉) · C. V. Ramu ·
K. Rasheed · Y. V. B. Sarma · G. V. M. Gupta
Centre for Marine Living Resources and Ecology, Ministry of Earth Sciences, Kochi 682508, India
e-mail: vish4well@gmail.com

V. Narayanan Nampoothiri S
School of Marine Sciences, Cochin University of Science and Technology, Kochi 682016, India

Introduction

Seasonally reversing winds and current patterns make the Arabian Sea unique in its physical processes, thereby influencing the biogeochemistry of the region. During winter monsoon (November to February), the wind blows from northeast leading to northward flow of West India Coastal Current (WICC) and during summer monsoon (June to September); wind blows from southwest leading to equatorward flow of WICC (Shetye et al., 1991, 1994) along the west coast of India. Poleward WICC carries low saline Bay of Bengal (BoB) waters to Arabian Sea during winter (Prasanna Kumar et al., 2004; Wyrtki, 1973) while equatorward WICC during summer carries Arabian Sea High Saline Water (ASHSW) southwards and to the BoB (Jain et al., 2017; Shetye et al., 1990) maintaining a salt balance in the north Indian Ocean. Both the winter and summer monsoons winds thereby lead to reversal of coastal currents (Kantha et al., 2008; Stramma et al., 1996). The low level jet streams blowing over May to September to the west coast of India were related to onset of southwest monsoon, monsoon rainfall and thereby the onset of coastal upwelling processes (Findlater, 1969).

Upwelling and convective mixing are the two major processes associated with the monsoons in the Arabian Sea. Winter cooling and subsequent convective mixing resulting in deepening the mixed layer in the NEAS were abundantly investigated by several researchers in the context of chlorophyll and primary productivity (Madhupratap et al., 1996; Prasanna Kumar et al., 2004; Shankar et al., 2016). Upwelling and related dynamics along the SEAS were studied by many authors (Banse, 1968; Rao & Joshi, 2008; Rao et al., 2005; Sharma, 1978) and explained that it was initiated by March from south and progressed towards north with maximum intensity during July/August. Gupta et al. (2016) observed that upwelling reaches the surface layer in May and declines by October with maximum intensity during June/July. Upwelling was initiated in the SEAS and propagates towards north with the northward propagating upwelling coastal Kelvin waves, and the cross-shore component of wind is instrumental in modifying the density structure in the surface layer, especially in the north (McCreary

et al., 1993; Shankar & Shetye, 1997; Smitha et al., 2008). Wind induced alongshore component makes upwelling dominant, and they observed upwelling and downwelling phases along the northwest and southeast regions of Findlater jet respectively (Muraleedharan & Kumar 1996). Coastal upwelling along the southwest coast of India is driven by offshore Ekman transport due to the alongshore wind, Ekman pumping, horizontal divergence of currents and by the propagation of coastally trapped waves, whereas downwelling along the coast is driven only by the convergence of currents and the propagation of coastally trapped Kelvin waves (Shah et al., 2015, 2019; Smitha et al., 2008, 2014; Vishnu et al., 2020). Other studies by Gopalakrishna et al. (2008) and Madhupratap et al. (2001) observed the time series upwelling phenomenon and indicated the SST cooling till post-monsoon, and they estimated high marine pelagic fish landings during summer monsoon. Narvekar et al. (2017) studied the stratification control on upwelling and its influence on pelagic fishery in the EAS. Several global studies on the upwelling dynamics and wind influence on the process have been covered in the recent years. The variabilities in upwelling favourable winds can affect ecosystem functioning (Chenillat et al., 2013). Abrahams et al. (2021) studied the wind and associated upwelling dynamics in the eastern boundary upwelling system using NOAA and ERA time series datasets. Xiu et al. (2018) studied alongshore wind induced upwelling and its control on stratification both in coastal and open ocean in the California current system. There are no studies on upwelling along the northwest coast (NEAS) during summer monsoon using in situ observations. However, Solanki et al. (2008) has analysed time series satellite observations in NEAS and stated that observed coastal upwelling along Okha extending up to Diu was due to the formation of a cyclonic eddy that enhanced the biological productivity of this region. Hareesh Kumar and Anand (2016) , Jayaram et al. (2010, 2012) and Jayaram and Kumar (2018) studied the upwelling related dynamics based on satellite and model technique and found that the Ekman transport due to alongshore winds, Ekman pumping due to wind stress curl, cyclonic eddy and southward WICC plays a major role in the upwelling and productivity patterns in the NEAS.

The present study aims to address the dynamics and forcing mechanisms of coastal upwelling and the time series chlorophyll distribution along northwest coast of India utilizing a large set of in situ data supplemented with satellite datasets. It will represent the first ever time series understanding of the complex physical processes operating in the NEAS. The first part deals with the time series variation of physical parameters. Time series chlorophyll distribution along the northwest coast was also addressed in this section. The possible forcing mechanisms of upwelling (wind and current) and the role of remote forcing were addressed in the next section of the paper. Brief comparison on the upwelling along northwest and southwest coast of India was also discussed in the final section.

## Data and methodology

Study area

Northern Arabian Sea is landlocked and is connected to two marginal seas, the Persian Gulf and the Red Sea which makes it much saltier. The continental shelf is narrow along the study region and has high velocity tidal fluctuations (Wagle, 1979). During the winter monsoon, winds are north easterly (Kantha et al., 2008), and during the summer monsoon, warm, moist air prevails, and a strong southwesterly wind jet runs diagonally across the Arabian Sea (Findlater, 1969). This general wind pattern associated with the monsoons results in the upper layer circulation. The coastal current driven by the pressure gradient (McCreary et al., 1993) is northward during winter monsoon and is southward during summer monsoon which are termed as the West India Coastal Current (WICC) (Shetye et al., 1990). Winter cooling is observed in the NEAS due to cold and dry northeasterly winds in the region during winter with subsequent convective mixing, thereby deepening the mixed layer and increasing the chlorophyll concentration (Madhupratap et al., 1996; Prasanna Kumar et al., 2004; Shankar et al., 2016). Excess evaporation and turbulent heat loss that cool the surface waters during winter lead to formation of Arabian Sea High Saline Watermass (ASHSW) in the study area (Kumar & Prasad, 1999). The weak

northerly winds and increased solar insolation during the inter-monsoon period lead to high SST and shallow mixed layer (Kumar & Prasad, 1996). Location map and sampling points along the northwest coast of India are shown in Fig. 1.

In situ data

The hydrographic data was collected during a series of repeat sampling conducted on board FORV Sagar Sampada and on board ORV Sagar Kanya during December 2017 to January 2019 which are used for this study. Data were collected from seven to ten cross-shore transects along the west coast of India in the eastern Arabian Sea as part of Marine Ecosystem Dynamics of Eastern Arabian Sea (MEDAS) programme, the first-ever monthly basin-scale study focused between 6–22°N and 77–67°E along the EAS. Observations were conducted covering coast-offshore transects (Okha and Veraval) at 10, 20, 30, 50, 75, 100, 200, 500, 1000 and 2000 m isobaths for the present study to understand the monthly variations in hydrography and dynamics.

The water temperature, salinity and chlorophyll were measured using a Seabird CTD (SBE 911 Plus)
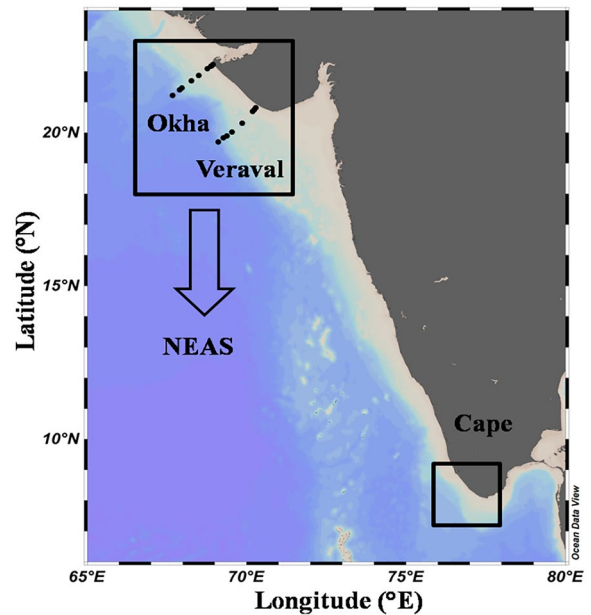
Fig. 1 Location map of study area along the northwest coast of India. This study focus on the Okha and Veraval transects in the NEAS (shown in box)

profiler with an accuracy of conductivity ± 0.0003 S/m, temperature ± 0.001 °C and pressure 0.015%. Water samples were collected using a Niskin samplers attached to the CTD Rosette, were analysed for salinity with a Guildline 8400 Autosal salinometer and were compared with CTD measured salinity and found to agree. The skin layer temperature was measured at each station using Navy bucket thermometer which has a range between -10 and 40 °C and an accuracy of ± 0.5 °C.

Satellite data

Sea surface temperature reprocessed product OSTIA (Good et al., 2020) provides daily gap-free maps of sea surface temperature (L4 product) at $0.05° \times 0.05°$ horizontal grid resolution, using in situ and satellite data. Datasets are downloaded from the following link https://resources.marine.copernicus.eu/product-download/SST_GLO_SST_L4_REP_OBSERVATIONS_010_011.

Wind data were derived from the IFREMER CERSAT Global Blended Mean Wind Fields that includes wind components (meridional and zonal), wind stress, wind/stress curl and divergence. The estimation of the 6-hourly blended wind products make use of all of the remotely sensed surface winds derived from scatterometers and radiometers available at this time and observation inputs for the objective method dealing with the calculation of 6-hourly wind fields over the global oceans. L4 winds are calculated from L2b products in combination with ERA interim wind analyses from January 1992 onwards. The analysis is performed for each synoptic time (00 h:00; 06 h:00; 12 h:00; 18 h:00 UTC) and with a spatial resolution of 0.25° in longitude and latitude over the global ocean (https://resources.marine.copernicus.eu/product-download/WIND_GLO_WIND_L4_REP_OBSERVATIONS_012_006).

Daily datasets on chlorophyll concentration based on the Copernicus-Glob Colour processor (L4 cloud free product) were considered from the following link https://resources.marine.copernicus.eu/product-download/OCEANCOLOUR_GLO_CHL_L4_REP_OBSERVATIONS_009_082. Products are based on the merging of the sensors SeaWiFS, MODIS, MERIS, VIIRS-SNPP&JPSS1 and OLCI-S3A&S3B and has a spatial resolution of 4 km.

Altimeter satellite gridded Sea Level Anomalies (SLA) and geostrophic currents with a spatial resolution of $0.25° \times 0.25°$ were computed with respect to a 20-year mean and were considered from https://resources.marine.copernicus.eu/product-download/SEALEVEL_GLO_PHY_L4_REP_OBSERVATIONS_008_047. The SLA is estimated by Optimal Interpolation, merging the measurement from the different altimeter missions. This product is processed by the DUACS multimission altimeter data processing system. It processes data from all altimeter missions: Jason-3, Sentinel-3A, HY-2A, Saral/AltiKa, Cryosat-2, Jason-2, Jason-1, T/P, ENVISAT, GFO and ERS1/2. The geostrophic currents are derived from SLA (geostrophic velocities anomalies, ugosa and vgosa variables) and from ADT (absolute geostrophic velocities, ugos and vgos variables). Monthly SLA maps were plotted to understand and track the propagation of coastally trapped upwelling/downwelling Kelvin waves in the EAS following the method by Rao et al. (2010).

Mass Ekman transport and pumping velocity

The Ekman transport is computed using bulk aerodynamic formulae based on Koracin et al. (2004) and Smith (1968):

$$M_E = \frac{\tau}{f}, \quad \tau = \rho_a C_d W^2 \tag{1}$$

where M_E represents mass Ekman transport, τ is the wind stress magnitude, ρ_a is the density of air (1.29 kg/m^3), C_d is the drag coefficient which varies with wind speed based on Large and Pond (1981) and Trenberth et al. (1990), W is the resultant magnitude of wind and f is the Coriolis parameter ($2\Omega Sin\Theta$, where Ω is the angular velocity of the earth that is 7.292×10^{-5} s^{-1} and Θ is the latitude).

Ekman pumping velocity (W_E) is calculated using Kraus and Businger (1994):

$$W_E = \frac{(\nabla \times \tau)}{\rho_w f} \tag{2}$$

where $\nabla \times \tau$ represents wind stress curl, ρ_w is the density of sea water (1025 kg/m^3) and f is the Coriolis parameter.

Results and discussion

Hydrography variation using in situ datasets

Monthly SST from the in situ observations using bucket thermometer were seen lowest (< 24 ℃) during December to February along the Okha and Veraval coast. SST gradually increases from March to about 29 ℃ by July. The warming phase was interrupted by mid-summer cooling off Okha and Veraval characterized by a drop in SST by about 4 ℃ (< 25.5 ℃) during July through September (Fig. S1a). This cooling phase halts with the establishment of secondary warming phase in October and November associated with downwelling and an increase in SST to about 28 ℃. The onset of winter conditions from December through February resulted in the drop in SST again. Thus, the SST showed bi-modal distribution with two peaks and two lows during a year. The development of coastal upwelling leading to mid-summer monsoon cooling along Okha and Veraval is clearly seen from the SST variation.

The vertical sections of temperature along the Okha transect showed colder waters (< 24 ℃) throughout the water column at coastal location (30-m depth) during winter (December to February). From March or early April, the temperature increases until July which is interrupted by a cooling due to upwelling during August–September when the temperature dropped to 25.5 ℃ (Fig. 2). By the end of September, the temperature increased with warmer conditions (28 ℃) extending from surface to bottom and later the effects of winter cooling

dominates from mid-November with a gradual fall of temperature (< 24 ℃). Salinity and density profiles also display significant shallowing during August–September from 30 m to surface. During the period of upwelling, the salinity was dropped (0.5 psu), and denser waters were uplifted, when compared to pre-monsoon and post-monsoon periods. The signature of coastal upwelling was stronger in the subsurface (below 20 m) compared to its surface expression. This indicates that upwelling process was weak at the northwest coast. Temperature profiles and the uplift of D24 and D26 isotherms from Fig. S1b confirm the presence of coastal upwelling observed during the summer monsoon period along the northwest coast. Time series vertical variation of temperature at shelf location (100-m depth) also shows signals of winter cooling associated cooler temperature and summer monsoon upwelling associated shallowing of cooler waters. This is also evident from the salinity and density profiles (Fig. 3).

During both the winter and summer monsoon, chlorophyll concentration was observed to be 2–3 mg/m^3 in the coastal station. Shelf region also showed high surface chlorophyll concentration during winter (0.5–0.75 mg/m^3) and summer (> 1 mg/m^3) monsoons, but the transition seasons were characterized by SCM (subsurface chlorophyll maxima) with 0.5–1 mg/m^3 at about 40–60-m depth. Study reveals that temperature and chlorophyll profiles show bi-modal peaks of high and low along the northwest coast. Lowering of temperature was due to the winter cooling (Madhupratap et al., 1996; Prasanna Kumar et al., 2004; Shankar et al., 2016) during winter monsoon and coastal

Fig. 2 Time series distribution of hydrographical parameters (temperature, chlorophyll, salinity and density) along the coastal waters (30 m) off Okha during Dec. 2017 to Jan. 2019
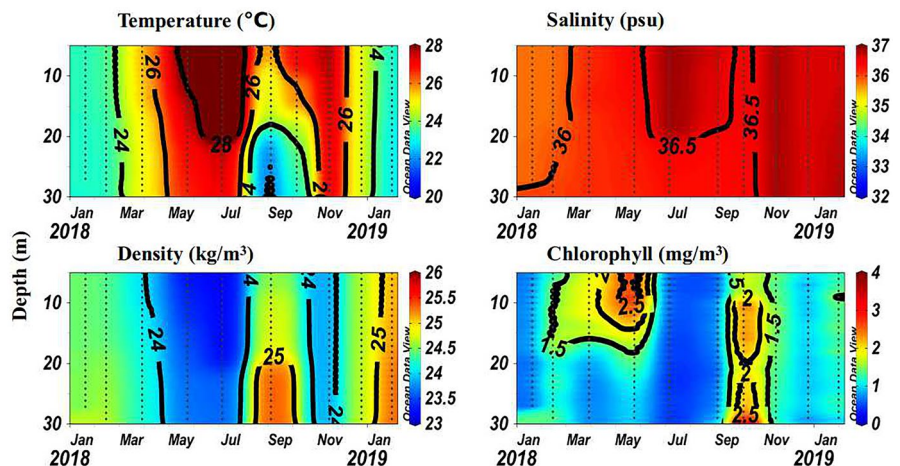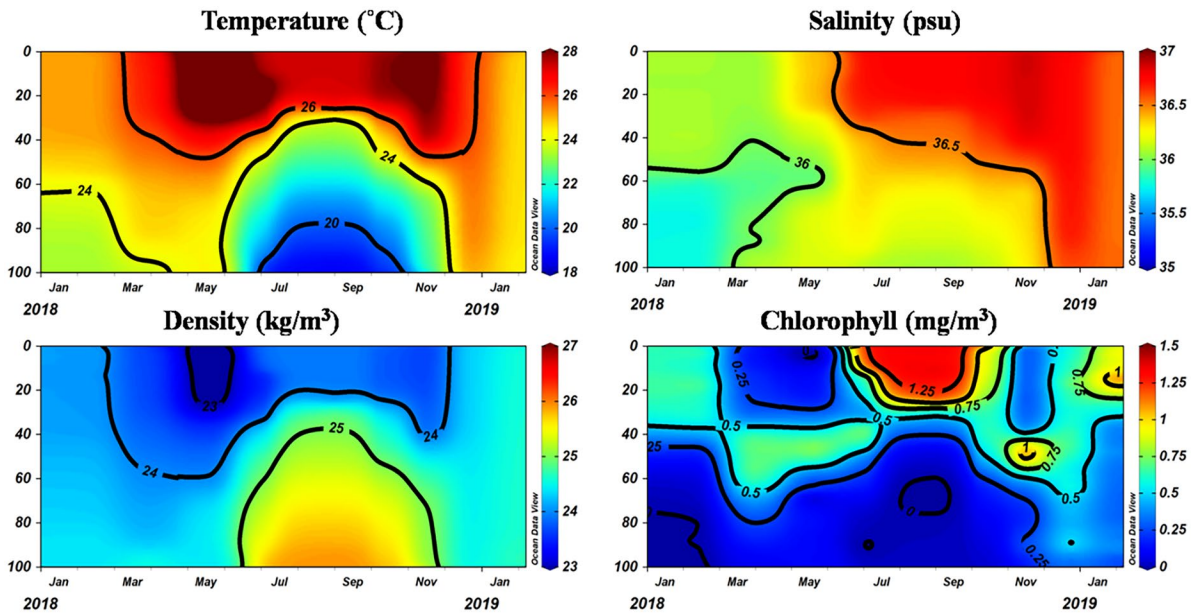
Fig. 3 Time series distribution of hydrographical parameters (temperature, chlorophyll, salinity and density) along the shelf waters (100 m) off Okha during Dec. 2017 to Jan. 2019

upwelling during summer monsoon, whereas the higher temperatures were observed in the spring and fall inter-monsoons. Shah et al. (2018) also observed chlorophyll peaks along the northwest during winter and summer monsoons and found that northwest coast of India were more productive throughout the year when compared to southwest coast of India. The peak winter cooling was observed during January to February and peak coastal upwelling during August to September, but the maximum production along the coast was observed during April–May and further during October. The maximum chlorophyll concentration (>2 mg/m^3) was observed with a lag after the peak winter cooling and upwelling along the coast, but along the shelf regions, associated cooling and high chlorophyll occurred simultaneously without a lag (Figs. 2, 3). The occurrence of recurring short-term eddies can trigger biological productivity during the spring inter monsoon after the peak winter cooling (Smitha et al., 2021). The lag in production may also be due to entrainment of nutrients held below the mixed layer to the euphotic zone (Vijith et al., 2016) giving rise to massive blooms during winter convection and re-establishment of mixed layer leading to high chlorophyll concentration after peak upwelling during summer monsoon. Jayaram et al. (2012) reported that

a fall in the wind stress magnitude followed by a high wind stress can lead to coastal shallowing of MLD and thereby lead to high productivity. This sudden rise and fall in wind stress can also lead to a lag in chlorophyll concentration.

Long-term variability

Time series satellite observations during 2012–2018 clearly reveal the decrease of SST during winter and mid-summer. The long-term observations during the 7-year period showed that during August–September (middle of summer monsoon) SST were comparatively high (26–27 °C) when compared to the December–February (winter monsoon) where it was less than 2 4°C. Thus, the inter-annual variability of SST about 22–30 °C possibly shows the combined influence of winds, currents and vertical processes in this region. This low SST along the coastal waters off northwest coast (Okha and Veraval) during summer monsoon is due to coastal upwelling, and this occurs to be a short-term and recurring process every year. The effect of winter cooling leads to very low SST (<24 °C) during December to February every year (Fig. 4). Negative SLA was observed along the coasts that may be attributed to

Fig. 4 SST (°C), SLA (m) and Chl (mg/m³) along the northwest region (box averaged 68–70°E and 20–23°N) during 2012 to 2018 showing short term and recurring upwelling process. Red box confirms upwelling signals during 2018
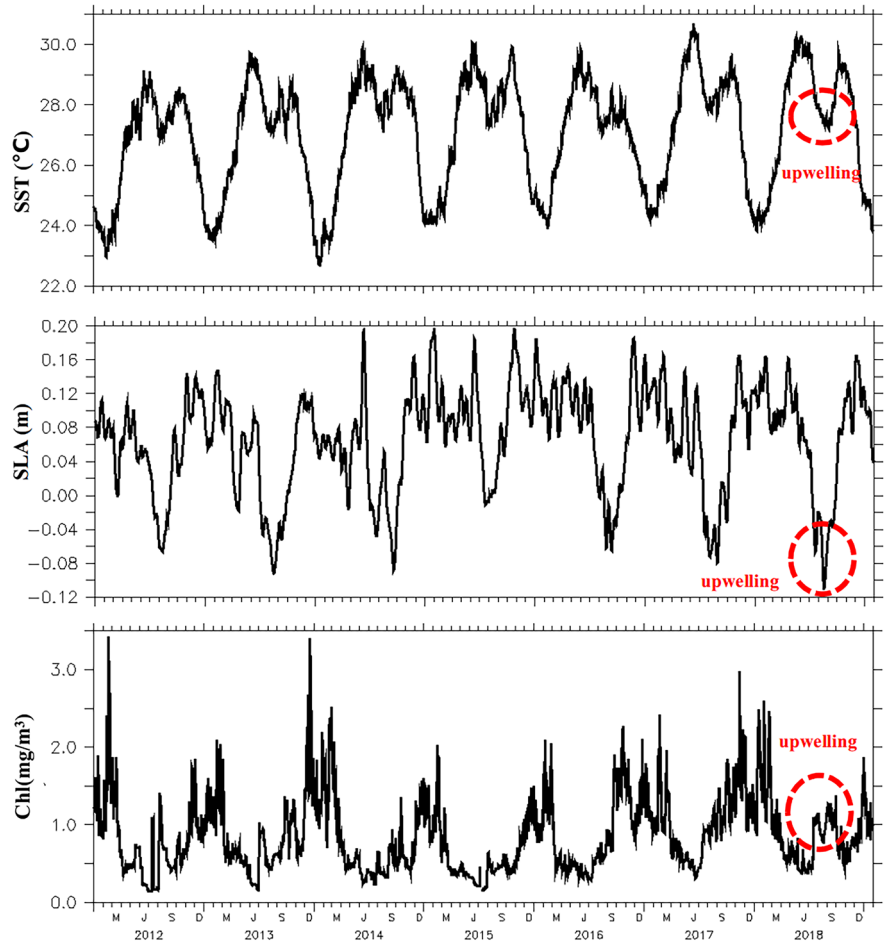

the coastal upwelling process. Time series chlorophyll pattern shows intense concentration (2–4 mg/m³) during winter monsoon (December to February) every year. During September–October, chlorophyll concentration ranges between 0.5 and 1.5 mg/m³ due to coastal upwelling. Northwest coast of India is found to be a productive region and can also lead to high marine fish landings during major seasons of the year due to combined effect of winter cooling and coastal upwelling compared to southwest coast. CMFRI (2019) annual report also mentioned off Gujarat coast with high marine fish landings compared to other coasts in India that supports this finding.

Monthly wind and current pattern

Winter season represents weak northerly/northeasterly winds with magnitude < 6 m/s along the northwest coast of India (Fig. S2). SLA shows high values with northward current during winter monsoon. Transition month (May) represents an increase in magnitude of wind ranging from 6 to 8 m/s with westerly to southwesterly direction. June to September (summer monsoon) represents a sharp increase in wind magnitude (8–12 m/s). Luther et al. (1990) and Muraleedharan and Kumar (1996) observed that strong southwest monsoon winds along the northwest region of Findlater jet lead to an increase in wind stress curl and upwelling. During August–September, we observed a change in wind pattern and magnitude (> 10 m/s) favouring upwelling along northwest (Fig. S2). This change in wind and associated current pattern may lead to the initiation of Ekman transport in the surface waters that leads to the formation of upwelling in the coastal region. Coastal orientation in the region also favours the offshore transport and upwelling. Jayaram et al. (2010) found that southwesterly monsoon winds
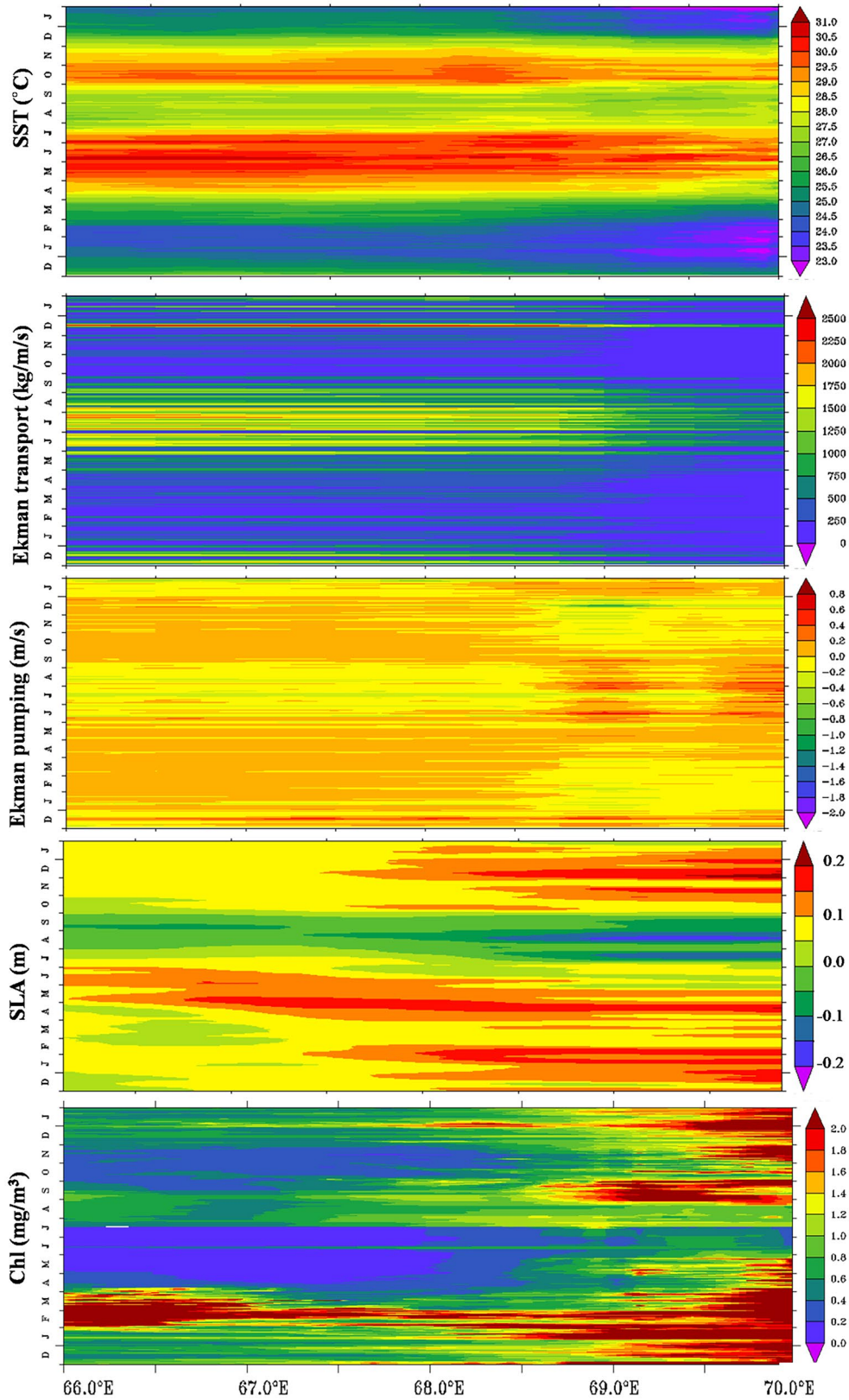
◀**Fig. 5** Time-longitude Hovmöller diagram of SST (℃), Ekman transport (kg/m/s), Ekman pumping (m/s), SLA (m) and Chl (mg/m^3) along the NEAS during 2018 averaged over 21–22.5°N

which are dominant during summer monsoon initiate upwelling; similar southwesterly winds were noticed in this observations along the northwest coast. SLA shows a drop (-0.1 m) along the study region similar to SEAS during summer monsoon and can be attributed to coastal upwelling. Here, the current flow shows a 45° tilt to right of the southwesterly winds, which drives southward coastal current (Fig. S3). Naidu (1999) also reported a shift of 45° in the wind pattern along the north and southwest coast of India when compared to central region. It is noticed that upwelling is declined by the month of October due to change in wind pattern to northerly and sudden decrease in magnitude to 4 m/s. Hence, it was found that combined effect of the varying wind and current pattern favours upwelling along the northwest.

Time series variation and forcing mechanism

Time-longitude Hovmöller diagram of SST (℃), Ekman transport (kg/m/s), Ekman pumping (m/s), SLA (m) and Chl (mg/m^3) for 2018 were considered to study the time series variation and forcing mechanism of coastal upwelling along the northwest region. SST ranged between 23 and 31℃ for the region with low values during winter monsoon (24 ℃) and summer monsoon (27–28 ℃), whereas it showed higher values (> 29 ℃) during spring and fall inter monsoons. Northwest coast shows bi-modal high and low SST over a year which is evident from Fig. 5. Winter cooling and associated lower SST (23 ℃) were found to be more intense along the coast (69–70°E) compared to offshore region (66–69°E) where comparatively high SST was observed (23–24℃). Signals of upwelling are evident from mid-July to September end extending from coast to offshore regions. Ekman transport for the region showed low values during the year except summer monsoon which is due to high wind stress. High values of Ekman transport (1000–2000 kg/m/s) is seen along the offshore region and is weaker towards coast. Ekman pumping due to wind stress curl showed positive values (0–0.8 m/s) in the coastal region compared to offshore (-0.2 to -0.4 m/s) where it is negative. This confirms Ekman

transport due to wind stress along the offshore region and Ekman pumping due to wind stress curl along the coastal region being the causative forcing factor for upwelling (Fig. 5). Possible role of remote forcing in the upwelling is confirmed from the negative SLA values (-0.1 to -0.2 m) during summer monsoon which shows the propagation of upwelling mode of Kelvin wave. Other seasons during the year showed positive values for SLA (0.1–0.2 m) indicating downwelling mode of Kelvin wave. Even though the wind conditions favoured upwelling from June, we could observe active upwelling with low SST during mid-July coinciding with the negative SLA (upwelling Kelvin wave) which proves the role of remote forcing in northwest coast upwelling (Fig. 5). The biological response for the northwest coast also showed bi-modal high and low chlorophyll associated with the seasons in the offshore regions. Intense chlorophyll was observed during winter and summer monsoons (> 1.5 mg/m^3) along the coast to offshore region. While the offshore regions exhibited bi-modal variation in chlorophyll concentration, the coastal regions remains productive throughout the year (Fig. 5). We also observed a lag between the peak chlorophyll concentration associated with winter cooling in the offshore region and upwelling process in the coastal region which is due to variation in wind stress.

Ekman dynamics

Ekman transport and pumping velocity are considered the proxy to upwelling/downwelling which affects the vertical movement of isotherms (Kok et al., 2017; Jacox et al., 2018). Ekman transport along a region depends on the magnitude and direction of the wind acting during northeast and southwest monsoon. During winter monsoon period, the wind direction is north-northeasterly (Prasanna Kumar & Prasad, 1996; Shetye et al., 1985). The low level Findlater jet blows towards west coast of India with high wind magnitude of 10–12 m/s during summer monsoon. Previous analysis showed that there exist varying Ekman dynamics along the coast and offshore region of northwest coast; hence, we computed Ekman transport and pumping velocities based on coast and offshore boxes. Kok et al. (2017) also found similar variabilities in Ekman transport and Ekman pumping controlling upwelling along the coastal regions in the South China Sea during southwest monsoon. The analysis shows that the

Table 1 Monthly averaged Mass Ekman transport (kg/m/s) and Ekman pumping velocity (m/s) along the coast and offshore regions of NEAS during 2018 (box averaged: coast, 69–70°E and 21–22.5°N, and offshore, 66–69°E and 21–22.5°N)

Month	Mass Ekman transport (M_E)		Ekman pumping velocity (W_E)	
	Coast	Offshore	Coast	Offshore
January	173.7	309	-1.06	0.002707
February	167.8	292	-0.8023	0.189
March	178.2	306	-0.5965	0.4921
April	206.9	363	0.05065	0.4572
May	359.6	669	0.3203	0.3206
June	**531.7**	**1021**	**1.349**	**-0.1572**
July	**814.8**	**1416**	**0.2726**	**-1.097**
August	**624.6**	**1059**	**0.8921**	**-0.8124**
September	**323.9**	**569**	**0.3656**	**0.2772**
October	112.7	203	-0.3124	0.2242
November	169.8	318	-0.5598	0.06293
December	342.8	646	-1.703	0.0282

Summer monsoon (June to September) values are highlighted as bold

value of Ekman transport is low in the coastal box but is comparatively higher along the offshore box for all the months. It shows maximum values during summer monsoon (June to September) (Table 1). Ekman transport is stronger with a magnitude of 1416 kg/m/s (offshore) and 814 kg/m/s (coastal) during July (summer monsoon). Positive values of Ekman pumping

velocity (>0.02 m/s) confirms the upwelling or vertical shift of isotherms to the surface in the coastal box during summer monsoon, whereas it is negative/weaker and shows signals of downwelling during other seasons (Table 1). Offshore box shows negative values for Ekman pumping during summer monsoon and positive values during other seasons. This confirms that Ekman transport drives upwelling in the offshore box and Ekman pumping drives upwelling in the coastal box (Table 1). The wind direction is always acting meridional along the coast; hence, the Ekman transport is offshore even in the winter monsoon along the EAS but has very less intensity (Shetye, 1984). Coastal orientation along northwest coast of India and high magnitude of wind stress play key role in controlling offshore Ekman transport and thereby the development of upwelling during the summer monsoon. This is similar to the observation reported in the SEAS by many authors (Shah et al., 2019; Smitha et al., 2008) off Cape region. The magnitude of wind stress is less during winter compared to summer monsoon. Positive Ekman pumping velocity during summer monsoon also favours coastal upwelling off northwest coastal regions off Okha and Veraval.

Role of remote forcing in the upwelling/downwelling along the west coast of India

Monthly SLA maps over the north Indian Ocean is considered to track the upwelling/downwelling mode of Kelvin wave. Kelvin waves are generated by


Fig. 6 Monthly propagation of upwelling mode of Kelvin wave along the Indian Ocean during 2018. Red box indicates signals of upwelling mode of Kelvin wave
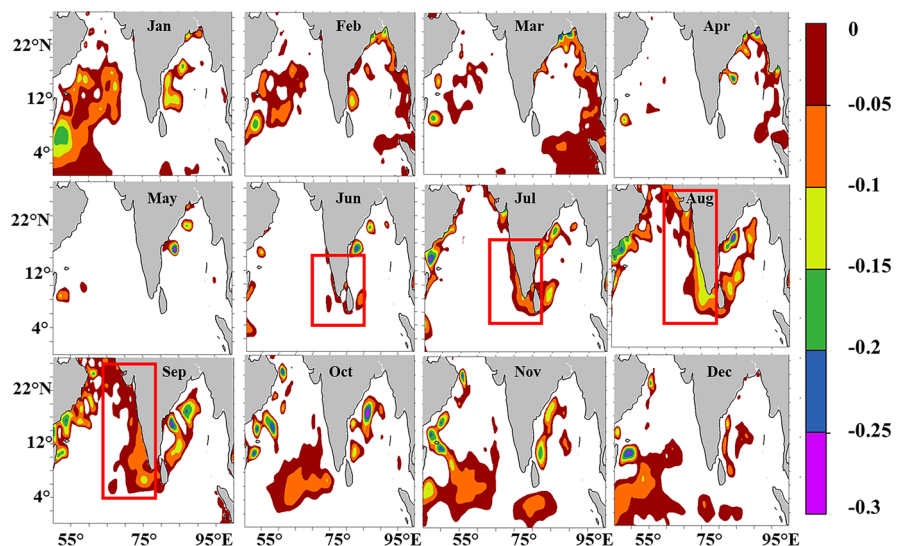
strong equatorial zonal winds and are trapped along the equator moving eastward, then along the coastal regions of BoB and turn around Sri Lanka to propagate poleward along west coast of India influencing both East India Coastal Current (EICC) and WICC (McCreary et al., 1993; Yu et al., 1991). Upwelling along the southwest coast of India is also driven by the offshore propagating Rossby waves generated by the coastally trapped Kelvin waves (Kumar et al., 2020; Shankar & Shetye, 1997; Smitha et al., 2008). Rao et al. (2010) proved that there are two alternate upwelling/downwelling modes of Kelvin waves propagating along the coastline of north Indian Ocean, but only one downwelling Kelvin wave reaches west coast during the months of October–November. Satellite data analysis to track the sea level anomaly shows a wave-like pattern generated from the Sri Lankan coast by May–June and propagates along the west coast of India (Fig. 6). This may be attributed to the

upwelling mode of Kelvin wave generated along the Sri Lankan coast due to strong tangential winds and is comparable to the study carried out by Gopalakrishna et al. (2008) and Hareesh Kumar and Anand (2016). When compared to the SEAS, along the central and northern part of EAS, the Kelvin wave shows less propagation and is restricted to the coast which is due to the high shelf width and strong cross-shore winds that are acting perpendicular to the coast as reported by Huthnance et al. (1986). There is a lag in the onset of upwelling observed from in situ datasets between south and north which coincides with the lag in propagation of this upwelling Kelvin wave. Similarly, the cessation of upwelling occurs early in the south and late in north, and this coincides with the downwelling mode of Kelvin wave which reaches during the months of October–November along the west coast (Fig. S4). This downwelling mode of Kelvin wave continues along the west coast of India except during

Fig. 7 SST (°C), wind stress (Pa) and Chl (mg/m³) distribution along the NEAS during 2018 (box averaged: 66–70°E and 21–22.5°N)
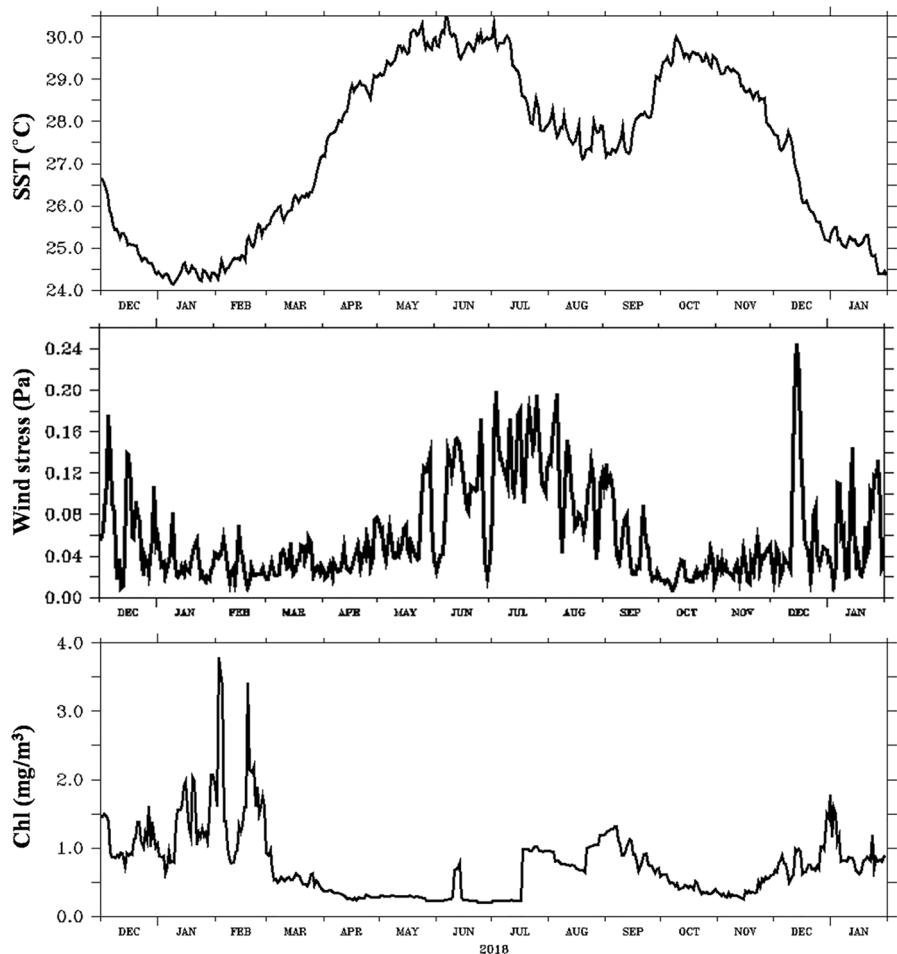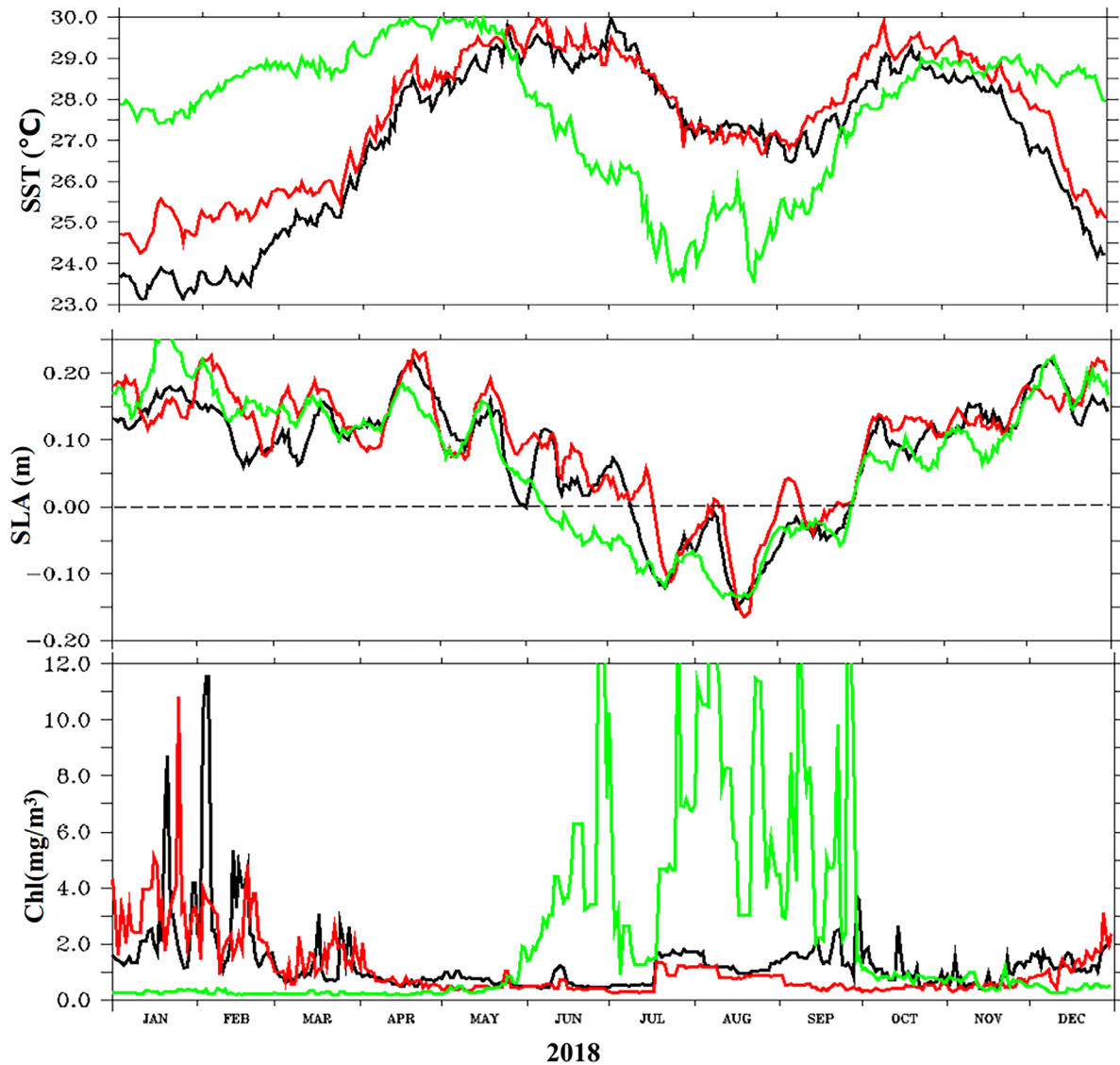
Fig. 8 SST ($^{\circ}$C), SLA(m) and Chl (mg/m^3) distribution along the coastal stations off Okha (black), Veraval (red) in the NEAS and Cape (green) in the SEAS during 2018 showing the variation of upwelling

June to September where upwelling mode of Kelvin wave was dominant.

Wind and chlorophyll

Time series data for the northwest region were used to study the relation between wind and chlorophyll. Lowering of SST during winter (December to February) and summer monsoons (July to September) due to winter cooling and upwelling was established from the previous sections and is also evident from

Fig. 7. The maximum wind stress was observed during December to January (0.12–0.16 Pa) and July to August (0.10–0.18 Pa). But chlorophyll concentration shows maximum values during February (2–4 mg/m^3) and September (1 mg/m^3). A lag of 10–20 days was observed between peak chlorophyll concentration and maximum wind stress in the study region during 2018 which is also observed from the in situ data (Fig. 7). Jayaram et al. (2012) also reported a two-weeks lag in maximum chlorophyll after occurrence of peak wind stress during

summer monsoon in the SEAS. This lag reported in the SEAS is also applicable in the northwest coast of India.

Comparison of upwelling along northwest and southwest coast of India

To compare the characteristics of upwelling along the NEAS and SEAS, we consider the two transects from the northwest region off Okha and Veraval and one along southwest coast off Cape. Time series in situ data showed a drop in temperature during summer monsoon along NEAS and SEAS. This cooling observed along NEAS is distinctly different from winter cooling which is more intense and associated with convective mixing during winter. The SST during upwelling period were warm at north (25.5 °C) compared to south (24 °C) (Fig. 8). In the SEAS, upwelling (D26) reached at surface in June, but in NEAS, it reached by August with nearly two months lag. However, the withdrawal of upwelling occurred in a short span of time, as it appeared to commence during early September in south compared to end of September in the north. It was understood that this lag in the onset and cessation of upwelling between NEAS and SEAS was due to the lag in propagation of upwelling/downwelling mode of Kelvin wave which was evident from SLA variation (Figs. 6, 8, S4). Chlorophyll data also shows high values during summer monsoon when there is a peak in upwelling. There is a lag in high chlorophyll and peak upwelling observed along NEAS, but this lag is missing in SEAS as the upwelling and high chlorophyll concentration occurs simultaneously (Fig. 8). This lag is observed in the NEAS is due to rise and fall in wind stress (Fig. 7) and matches with findings of Jayaram et al. (2012) which shows relation between wind stress and lag in productivity. From this study, it is inferred that a lag of two month in the onset of upwelling between SEAS and NEAS but cessation occurs in a very short span of time.

Conclusions

Upwelling in the NEAS is observed to be recurring, but short term during August–September. SST along NEAS is warmer (25.5 °C) when compared to SEAS (24 °C). It is apparent that the change in wind and current pattern is the major causative factor for the development of upwelling. In the northwest coast of India, coastal orientation also favours the change of wind pattern leading to coastal upwelling. Rise and fall observed in the wind stress and southward directing coastal current during southwest monsoon triggers uplift of isotherms along the northwest. Remote forcing also plays a major role in the upwelling/downwelling processes in this region. The upwelling mode of Kelvin wave formed due to strong tangential winds along the Sri Lanka coast propagates northward along the west coast which is initiated during May–June and propagates up to September and downwelling mode of Kelvin wave propagating from equatorial region through Bay of Bengal reaches west coast by October coinciding with the withdrawal of southwest monsoon. This upwelling/downwelling mode of Kelvin wave and southwest monsoon winds plays a major role in the late onset and cessation of upwelling along the NEAS compared to SEAS. Coastal region of NEAS remains productive throughout the year due to the combined effect of coastal upwelling during summer monsoon and winter cooling during winter monsoon. High chlorophyll along the NEAS occurs with a lag after the peak winter cooling and upwelling, and this is due to sudden rise and fall in wind stress. There was a delay of about two months between the onset of upwelling in south and north in EAS as indicated by drop in SST. However, the cessation of upwelling occurred in a short span of time, as it appeared to commence during early September in SEAS compared to end of September or early October along the NEAS. Hence, it can be concluded from this work and other previous studies related to upwelling that the entire EAS shows signals of coastal upwelling but with different forcing mechanisms and is not restricted to SEAS. But off Mumbai, it was weak and restricted to subsurface due to bathymetry/shelf break changes and also due to strong cross-shore winds which are perpendicular to the coast. This work brings a better understanding to the upwelling process along the EAS and to give a light to the description of the other ecosystem response/processes in the northwest coast of India.

during sampling on board. This is the CMLRE contribution No.146

Data availability The datasets generated are deposited in the repository of CMLRE and can be made available upon reasonable request.

Declarations

Conflict of interest The authors declare no competing interests.

References

Abrahams, A., Schlegel, R. W., & Smit, A. J. (2021). Variation and change of upwelling dynamics detected in the world's eastern boundary upwelling systems. *Frontiers in Marine Science, 8,* 626411. https://doi.org/10.3389/fmars.2021.6264

Banse, K. (1968). Hydrography of the Arabian Sea shelf of India and Pakistan and effects on demersal fishes. *In Deep sea research and oceanographic Abstracts, 15*(1)*,* 45–79. Elsevier.

Chenillat, F., Rivière, P., Capet, X., Franks, P. J., & Blanke, B. (2013). California coastal upwelling onset variability: Cross-shore and bottom-up propagation in the planktonic ecosystem. *PLoS One, 8*(5), e62281.

CMFRI. (2019). CMFRI Annual Report 2018–19.

Findlater, J. (1969). A major low-level air current near the Indian Ocean during the northern summer. *Quarterly Journal of the Royal Meteorological Society, 95*(404), 362–380.

Good, S., Fiedler, E., Mao, C., Martin, M. J., Maycock, A., Reid, R., et al. (2020). The current configuration of the OSTIA system for operational production of foundation sea surface temperature and ice concentration analyses. *Remote Sensing, 12,* 720. https://doi.org/10.3390/rs12040720

Gopalakrishna, V. V., Rao, R. R., Nisha, K., Girishkumar, M. S., Pankajakshan, T., Ravichandran, M., & Rajesh, S. (2008). Observed anomalous upwelling in the Lakshadweep Sea during the summer monsoon season of 2005. *Journal of Geophysical Research: Oceans, 113*(C5).

Gupta, G. V. M., Sudheesh, V., Sudharma, K. V., Saravanane, N., Dhanya, V., Dhanya, K. R., & Naqvi, S. W. A. (2016). Evolution to decay of upwelling and associated biogeochemistry over the southeastern Arabian Sea shelf. *Journal of Geophysical Research: Biogeosciences, 121*(1), 159–175.

Hareesh Kumar, P. V., & Anand, P. (2016). Coastal upwelling off the southwest coast of India: Observations and simulations. *International Journal of Digital Earth, 9*(12), 1256–1274.

Huthnance, J. M., Mysak, L. A., & Wang, D. P. (1986). Coastal trapped waves. *Baroclinic Processes on Continental Shelves, 3*, 1–18.

Jacox, M. G., Edwards, C. A., Hazen, E. L., & Bograd, S. J. (2018). Coastal upwelling revisited: Ekman, Bakun, and improved upwelling indices for the US West Coast. *Journal of Geophysical Research: Oceans, 123*(10), 7332–7350.

Jain, V., Shankar, D., Vinayachandran, P. N., Kankonkar, A., Chatterjee, A., Amol, P., & Fernandes, R. (2017). Evidence for the existence of Persian Gulf water and Red Sea water in the Bay of Bengal. *Climate Dynamics, 48*(9–10), 3207–3226.

Jayaram, C., & Kumar, P. D. (2018). Spatio-temporal variability of upwelling along the southwest coast of India based on satellite observations. *Continental Shelf Research, 156*, 33–42.

Jayaram, C., Chacko, N., Joseph, K. A., & Balchand, A. N. (2010). Interannual variability of upwelling indices in the Southeastern Arabian Sea: A satellite based study. *Ocean Science Journal, 45*(1), 27–40.

Jayaram, C., Udaya, B. T., Ajith, J. K., & Balchand, A. N. (2012). Application of satellite products to study upwelling, chlorophyll and mixed layer depth of Southeastern Arabian Sea. *The International Journal of Ocean and Climate Systems, 3*(2), 97–108.

Kantha, L., Rojsiraphisal, T., & Lopez, J. (2008). The North Indian Ocean circulation and its variability as seen in a numerical hindcast of the years 1993–2004. *Progress in Oceanography, 76*(1), 111–147.

Kok, P. H., Mohd Akhir, M. F., Tangang, F., & Husain, M. L. (2017). Spatiotemporal trends in the southwest monsoon wind-driven upwelling in the southwestern part of the South China Sea. *PLoS one, 12*(2), e0171979.

Koračin, D., Dorman, C. E., & Dever, E. P. (2004). Coastal perturbations of marine-layer winds, wind stress, and wind stress curl along California and Baja California in June 1999. *Journal of Physical Oceanography, 34*(5), 1152–1173.

Kraus, E. B., & Businger, J. A. (1994). *Atmosphere-ocean interaction, 27*. Oxford University Press.

Kumar, K. V., Rasheed, K., Smitha, B. R., Nampoothiri, S. V. N., & Sudhakar, M. (2020). Description on variability of shelf-edge hydrography and current structure of the South Eastern Arabian Sea during summer and winter monsoons. *Environmental Monitoring and Assessment, 192*(11), 1–22.

Kumar, S. P., & Prasad, T. G. (1996). Winter cooling in the northern Arabian Sea. *Current Science, 71*(11), 834–841.

Kumar, S. P., & Prasad, T. G. (1999). Formation and spreading of Arabian Sea high-salinity water mass. *Journal of Geophysical Research: Oceans, 104*(C1), 1455–1464.

Large, W. G., & Pond, S. (1981). Open ocean momentum flux measurements in moderate to strong winds. *Journal of Physical Oceanography, 11*(3), 324–336.

Luther, M. E., O'Brien, J. J., & Prell, W. L. (1990). Variability in upwelling fields in the northwestern Indian Ocean 1. Model experiments for the past 18,000 years. *Paleoceanography, 5*(3), 433–445.

Madhupratap, M., Kumar, S. P., Bhattathiri, P. M. A., Kumar, M. D., Raghukumar, S., Nair, K. K. C., & Ramaiah, N. (1996). Mechanism of the biological response to

winter cooling in the northeastern Arabian Sea. *Nature, 384*(6609), 549–552.

Madhupratap, M., Nair, K. N. V., Gopalakrishnan, T. C., Haridas, P., Nair, K. K. C., Venugopal, P., & Gauns, M. (2001). Arabian Sea oceanography and fisheries of the west coast of India. *Current Science, 81*(4), 355–361.

McCreary, J. P., Jr., Kundu, P. K., & Molinari, R. L. (1993). A numerical investigation of dynamics, thermodynamics and mixed-layer processes in the Indian Ocean. *Progress in Oceanography, 31*(3), 181–244.

Muraleedharan, P. S., & Kumar, S. P. (1996). Arabian Sea upwelling–a comparison between coastal and open ocean regions. *Current Science, 71*, 842–846.

Naidu, P. D., Kumar, M. R., & Babu, V. R. (1999). Time and space variations of monsoonal upwelling along the west and east coasts of India. *Continental Shelf Research, 19*(4), 559–572.

Narvekar, J., D'Mello, J. R., Prasanna Kumar, S., Banerjee, P., Sharma, V., & Shenai-Tirodkar, P. (2017). Winter-time variability of the eastern Arabian Sea: A comparison between 2003 and 2013. *Geophysical Research Letters, 44*(12), 6269–6277.

Prasanna Kumar, S., Narvekar, J., Kumar, A., Shaji, C., Anand, P., Sabu, P., & Nair, K. K. C. (2004). Intrusion of the Bay of Bengal water into the Arabian Sea during winter monsoon and associated chemical and biological response. *Geophysical Research Letters, 31*(15).

Prasanna Kumar, S., & Prasad, T. G. (1996). Winter cooling in the northern Arabian Sea. *Current Science, 71*, 834–841.

Rao, A. D., & Joshi, M. (2008). Modelling of upwelling processes during pre-monsoon and monsoon along the west coast of India. *International Journal of Ecology and Development, 10,* S08.

Rao, A. D., Joshi, M., & Babu, S. V. (2005). A three-dimensional numerical model of coastal upwelling along the west coast of India. *Mathematical and Computer Modelling, 41*(2–3), 177–195.

Rao, R. R., Kumar, M. G., Ravichandran, M., Rao, A. R., Gopalakrishna, V. V., & Thadathil, P. (2010). Interannual variability of Kelvin wave propagation in the wave guides of the equatorial Indian Ocean, the coastal Bay of Bengal and the southeastern Arabian Sea during 1993–2006. *Deep Sea Research Part I: Oceanographic Research Papers, 57*(1), 1–13.

Shah, P., Sajeev, R., & Gopika, N. (2015). Study of upwelling along the west coast of India—A climatological approach. *Journal of Coastal Research, 31*(5), 1151–1158.

Shah, P., Sajeev, R., Santhosh, K. M., Thara, K. J., Muhammad, S., John, K. L., & George, G. (2018). Observed signals of upwelling and downwelling along the west coast of India. *Indian Journal of Geo-Marine Sciences, 47*(3), 604–612.

Shah, P., Sajeev, R., Thara, K. J., George, G., Shafeeque, M., Akash, S., & Platt, T. (2019). A holistic approach to upwelling and downwelling along the south-west coast of India. *Marine Geodesy, 42*(1), 64–84.

Shankar, D., & Shetye, S. R. (1997). On the dynamics of the Lakshadweep high and low in the southeastern Arabian Sea. *Journal of Geophysical Research: Oceans, 102*(C6), 12551–12562.

Shankar, D., Remya, R., Vinayachandran, P. N., Chatterjee, A., & Behera, A. (2016). Inhibition of mixed-layer deepening during winter in the northeastern Arabian Sea by the West India Coastal Current. *Climate Dynamics, 47*(3–4), 1049–1072.

Sharma, G. S. (1978). Upwelling off the southwest coast of India. *Indian Journal of Marine Sciences, 7*(4), 209–218.

Shetye, S. R. (1984). Seasonal variability of the temperature field off the south-west coast of India. *The Proceedings of the Indian Academy of Sciences: Earth and Planetary Sciences, 93*, 399–411.

Shetye, S. R., Shenoi, S. S. C., Antony, M. K., & Krishna Kumar, V. (1985). Monthly - mean wind stress along the coast of the north Indian Ocean. *The Proceedings of the Indian Academy of Sciences: Earth and Planetary Sciences, 94*, 129–137.

Shetye, S. R., Gouveia, A. D., Shenoi, S. S. C., Michael, G. S., Sundar, D., Almeida, A. M., & Santanam, K. (1991). The coastal current off western India during the northeast monsoon. *Deep Sea Research: Part A, 38,* 1517–1529.

Shetye, S. R., Gouveia, A. D., & Shenoi, S. S. C. (1994). Circulation and water masses of the Arabian Sea. *Proceedings of the Indian Academy of Sciences-Earth and Planetary Sciences, 103*(2), 107–123.

Shetye, S. R., Gouveia, A. D., Shenoi, S. S. C., Sundar, D., Michael, G. S., Almeida, A. M., & Santanam, K. (1990). Hydrography and circulation off the west coast of India during the southwest monsoon 1987. *Journal of Marine Research, 48*(2), 359–378.

Smith, R. L. (1968). Upwelling. *Oceanography and Marine Biology, Annual Review, 6*, 11–46.

Smitha, A., Joseph, K. A., Jayaram, C., & Balchand, A. N. (2014). Upwelling in the southeastern Arabian Sea as evidenced by Ekman mass transport using wind observations from OCEANSAT–II Scatterometer. *Indian Journal of Geo-Marine Sciences, 43*(01), 111–116.

Smitha, B. R., Sanjeevan, V. N., Padmakumar, K. B., Midhun, S. H., Salini, T. C., & Lix, J. K. (2021). Role of mesoscale eddies in the sustenance of high biological productivity in North Eastern Arabian Sea during the winter-spring transition period. *Science of the Total Environment, 151173*, 0048–9697. https://doi.org/10.1016/j.scitotenv.2021.151173

Smitha, B. R., Sanjeevan, V. N., Vimalkumar, K. G., & Revichandran, C. (2008). On the upwelling off the southern tip and along the west coast of India. *Journal of Coastal Research, 24*, 95–102.

Solanki, H. U., Mankodi, P. C., Dwivedi, R. M., & Nayak, S. R. (2008). Satellite observations of main oceanographic processes to identify ecological associations in the Northern Arabian Sea for fishery resources exploration. *Hydrobiologia, 612*(1), 269.

Stramma, L., Fischer, J., & Schott, F. (1996). The flow field off southwest India at 8N during the southwest monsoon of August 1993. *Journal of Marine Research, 54*(1), 55–72.

Trenberth, K. E., Large, W. G., & Olson, J. G. (1990). The mean annual cycle in global ocean wind stress. *Journal of Physical Oceanography, 20*(11), 1742–1760.

Vijith, V., Vinayachandran, P. N., Thushara, V., Amol, P., Shankar, D., & Anil, A. C. (2016). Consequences of inhibition of mixed-layer deepening by the West India Coastal Current for winter phytoplankton bloom in

the northeastern Arabian Sea. *Journal of Geophysical Research: Oceans, 121*(9), 6583–6603.

Vishnu, N. N. S., Sachin, T. S., & Rasheed, K. (2020). Dynamics and forcing mechanisms of upwelling along the south eastern Arabian sea during south west monsoon. *Regional Studies in Marine Science, 40*, 101519. https://doi.org/10.1016/j.rsma.2020.101519

Wagle, B. G. (1979). Geomorphology of the Gulf of Kutch. *Indian Journal of Marine Sciences, 8*(3), 123–126.

Wyrtki, K. (1973). Physical oceanography of the Indian Ocean. *In The biology of the Indian Ocean,* pp. 18–36. Springer, Berlin, Heidelberg.

Xiu, P., Chai, F., Curchitser, E. N., & Castruccio, F. S. (2018). Future changes in coastal upwelling ecosystems with global warming: The case of the California Current System. *Scientific Reports, 8*(1), 1–9.

Yu, L., O'Brien, J. J., & Yang, J. (1991). On the remote forcing of the circulation in the BoB. *Journal of Geophysical Research, 96*(C11), 449–454.